PERGAMON

International Journal of Multiphase Flow 26 (2000) 1875–1889

International Journal of Multiphase Flow

www.elsevier.com/locate/ijmulflow

Time-dependent pattern formation for convection in two layers of immiscible liquids

Y.Y. Renardy*, C.G. Stoltz

Department of Mathematics, Virginia Polytechnic Institute and State University, Blacksburg, VA 24061-0123, USA

Received 1 July 1999; received in revised form 24 November 1999

Abstract

A linear and weakly nonlinear stability analysis is performed for specific two-layer systems which have been examined experimentally in the past for purely buoyancy driven convection. Time-dependent oscillations arise at the first onset of instability. For the water/silicone oil system, oscillations are predicted for a range of wavelengths and depth fractions. For the Fluorinert/silicone oil system, oscillations are theoretically predicted in a very narrow parameter range. A 3D Hopf bifurcation on a hexagonal lattice is investigated for time-periodic patterns that arise at onset in extended domains. In both fluid systems, travelling rolls, wavy rolls of type 1, and oscillating triangles are stable for most regimes.

Keywords: Double-layer convection; Pattern formation; Hopf bifurcation; Buoyancy-driven convection

1. Introduction

Two-layer systems heated from below have been investigated experimentally by Degen et al. (1998). Marangoni effects are not relevant to the experimental conditions discussed, and purely buoyancy driven convection is studied. Time-periodic oscillations were observed in rectangular and annular channels. The presence of the interface and the coupling between the fluids has generated interest in this problem from both experimentalists and theoreticians (Busse and Sommermann, 1996; Gershuni and Zhukhovitskii, 1976; Johnson and Narayanan, 1997, 1998; Fujimura and Renardy, 1995; Johnson et al., 1998).

* Corresponding author.

PII: S0301-9322(99)00117-2

Fig. 1 is a sketch of the system geometry. In our theoretical treatment, the system is unbounded in the horizontal directions. Distance is nondimensionalized with respect to plate separation l^* and time with l^{*2}/κ_1 where κ_1 is the thermal diffusivity of the lower liquid. The average value of the interface height is denoted l_1. At the temperature of the top plate, each fluid has coefficient of cubical expansion $\hat{\alpha}_i$, thermal diffusivity κ_i, thermal conductivity k_i, viscosity μ_i, density ρ_i, and kinematic viscosity $\nu_i = \mu_i/\rho_i$. In each fluid, the governing equations are the heat transport equation and the Navier–Stokes equations with the Oberbeck–Boussinesq approximation. At the interface, we have: the continuity of velocity, temperature, heat flux and shear stress; the jump in the normal stress is balanced by interfacial tension and curvature; and the kinematic free surface condition holds. There are six dimensionless ratios arising from the fluid properties: $m = \mu_1/\mu_2$, $r = \rho_1/\rho_2$, $\gamma = \kappa_1/\kappa_2$, $\zeta = k_1/k_2$, $\beta = \hat{\alpha}_1/\hat{\alpha}_2$ and $l_1 = l_1^*/l^*$. We define a Rayleigh number $R = g\hat{\alpha}_1\Delta T l^{*3}/(\kappa_1\nu_1)$, a Prandtl number $P = \nu_1/\kappa_1$, and an interfacial tension parameter $S = S^* l^*/(\kappa_1\mu_1)$, where S^* is the dimensional interfacial tension.

The base state for the system is given by a flat interface at $z = l_1$, a zero velocity field and a temperature field which varies linearly with z in each fluid. Equations governing linearized perturbations proportional to $\exp(i\alpha x + \sigma t)$, and the full equations required for a bifurcation analysis are given in Chapter III of Joseph and Renardy (1993). We shall apply this to our situation where oscillations are excited by a competition between the bulk motions in each fluid, with the interface remaining approximately flat (Busse and Sommermann, 1996; Degen et al., 1998; Rasenat et al., 1989; Andereck et al., 1996, 1998; Renardy and Stoltz, 1999; Renardy, 1996a,b; Colinet and Legros, 1994). These time-periodic states emerge at onset, and not as secondary bifurcations. The fluids were chosen by Degen et al. (1998) to satisfy two conditions. First, the effective Rayleigh numbers of the fluids must be equal. These are $R_1 = g\hat{\alpha}_1\Delta T_1 l_1^{*3}/(\kappa_1\nu_1)$, and $R_2 = g\hat{\alpha}_2\Delta T_2 l_2^{*3}/(\kappa_2\nu_2)$, $l_2^* = l^* - l_1^*$. The continuity of heat flux across the interface fixes the ratio $\Delta T_1/\Delta T_2$ to be $l_1/(\zeta l_2)$. Using this, the ratio R_1/R_2 is $(\beta r)/(\zeta m\gamma a^4)$, where $a = l_2/l_1$. When this ratio is approximately 1, an oscillatory onset is intuitively expected. This yields the depth ratio $a = [(\beta r)/(\zeta m\gamma)]^{1/4}$. However, Renardy (1996b) has shown that this condition alone is not sufficient for exciting time-periodic states, and a second condition

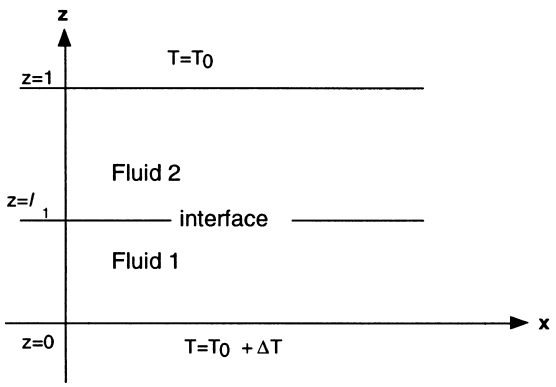

Fig. 1. Problem definition in 3D. The y-axis extends into the paper. Walls are situated at $z = 0$ with temperature $T_0 + \Delta T$ and at $z = 1$ with temperature T_0. The unperturbed interface separating fluid 1 and fluid 2 is at $z = l_1$.

required of the system is that it be sufficiently far from self-adjoint. For large Prandtl numbers and a non-deformable interface, it is shown that when $\gamma\beta r = 1$, the onset is steady. Therefore, oscillations are more likely to be found when this combination moves farther away from 1. These criteria led to the choice of two fluid pairs: a layer of Fluorinert lying below a layer of silicone oil 47v10, and silicone oil 47v2 lying over water. The properties of these fluids are given by Andereck et al. (1996, 1998) and Degen et al. (1998).

For the Fluorinert/silicone oil system, the effective Rayleigh numbers are balanced when the dimensionless lower liquid depth is approximately 0.43. For this system, $\gamma\beta r$ is 0.776, and steady onsets were observed (Degen et al., 1998; Andereck et al., 1996). As the temperature difference was increased in the experiments, the roll motion became irregular, and the velocity became time-dependent in the range $0.357 \leq l_1 \leq 0.382$ at a ΔT roughly 0.1°C above the primary steady onset. The period of the time-dependent state was approximately 50 min at low ΔT. The wavelength of the pattern was found to be roughly 14.7 mm, or dimensionless wave number $\alpha = 5.2$. Linear theory predicts that Hopf modes (time-periodic oscillations) occur at dimensionless lower liquid depth 0.43 with periods of 50 min or longer, reminiscent of the periods in the experiments. The weakly nonlinear theory predicts saturation in the form of traveling rolls (Renardy, 1996b).

Since oscillations were not observed at onset for the Fluorinert/silicone oil system, a search was conducted for another fluid pair, for which oscillations would occur over a wider range of liquid depths. The guiding quantity was to make $\gamma\beta r$ as far away from 1 as possible. This led to the choice of the water/silicone oil system (Degen, 1997). The linear theory in this paper details this fluid pair, for which the experimental data were more recently investigated. Time-dependent onsets were indeed observed experimentally for the depths predicted by linear theory (see Section 2). However, the periods and wave numbers do not correspond.

While the experimental observation of oscillations over a wide range of lower liquid depths may appear to indicate that the water/silicone oil system is a superior pairing for examination, the choice of fluid pair is complicated by the difficulty in measuring and observing the system. The advantage of the Fluorinert/silicone oil system and the disadvantage of the water/silicone oil system are discussed by Degen et al. (1998).

2. Linear stability

2.1. The water/silicone oil 47v2 system

The parameters are $P = 7.1$, $r = 1.149$, $m = 0.576$, $\beta = 0.1766$, $\zeta = 5.44$, $\gamma = 1.845$, and $S^* = 52.5$ dyn/cm (Degen, 1997). Balancing the Rayleigh numbers yields $l_1 = 0.7$, and $\gamma\beta r = 0.374$. Fig. 20 of Degen et al. (1998) shows the temperature differences at depths 0.60, 0.67 and 0.71 for oscillatory onsets to be 0.62, 0.68, and 0.70°C, respectively, and these conditions are above the theoretically predicted criticality. Fig. 22 of Degen et al. (1998) shows the periods and wave numbers observed in the top layer, for lower liquid depth $l_1 = 0.71$: wavenumber $\alpha = 11.6$, and periods corresponding to $\mathrm{Im}\,\sigma = 3.5$–4.6.

2.1.1. Neutral stability curves

Fig. 2 shows the trends in the critical Rayleigh number vs. wave number, and Fig. 3 shows the $\mathrm{Im}\,\sigma$ vs. wave number, for dimensionless lower fluid depths $l_1 = 0.62$–0.71. The neutral stability curves show possible time-periodic states in the range of wave numbers roughly 2 to 6. The troughs of the curves are rather flat over many wave numbers, and the tendency from depth 0.6 to 0.69 is that a wave number larger than 5 is the onset mode, while there is a switch at depth 0.7, and the wave number less than 5 becomes the onset mode. This switch occurs because the curve develops two lobes in the presence of the Hopf modes, with one lobe descending and the other rising. The depth ratio 0.7 is unique in that the troughs of the neutral stability curve hit two wave numbers at approximately a 2:1 ratio. This is the depth ratio where experimental data were taken, and we would expect to see resonances and complicated dynamics over many wave numbers. At the other depth ratios, the onset mode is steady, but the Hopf modes exist at Rayleigh numbers very close to that of the onset mode. The critical Rayleigh numbers and wavenumbers are shown in Fig. 4 for each depth l_1.

The shortest periods are around 26 min ($\mathrm{Im}\,\sigma = 4$) at $l_1 = 0.66$ and wavelength 22 mm (wave number 3.5). The period at $l_1 = 0.7$ and wavelength 13 mm (wave number 5.7) is 70 min ($\mathrm{Im}\,\sigma = 1.5$). Measurements reported by Degen et al. (1998) at depth fraction 0.71 are shown in their Figs 21 and 22. They show plots of period vs. ΔT and wave number vs. ΔT for ΔT from roughly 0.7 to 2°C. The lowest value of ΔT which they record corresponds to Rayleigh numbers just above 20,000 and we see from Fig. 2 that for a Rayleigh number of 20,000, many wave numbers are already unstable. Experimental data in Fig. 20 of Degen et al. (1998) show the critical values of ΔT at lower liquid depths 0.6, 0.67 and 0.71 which give Rayleigh numbers 19,000, 20,800 and 21,500, respectively. Comparing with the neutral stability curves in Figs. 2

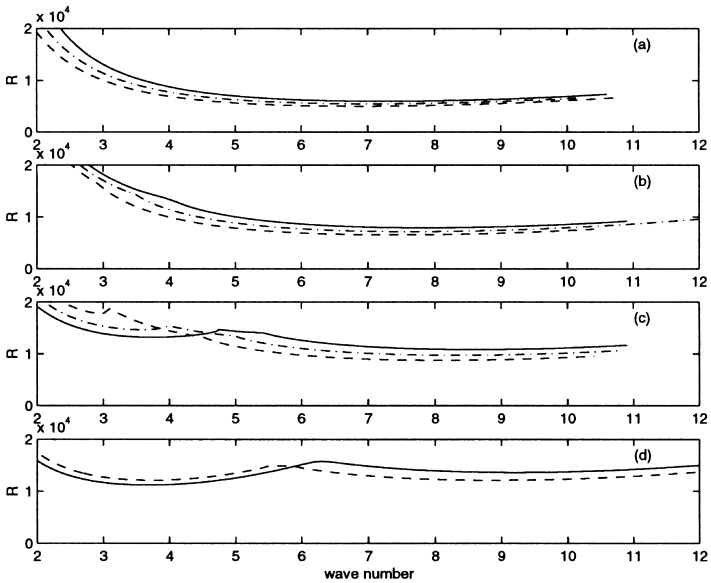

Fig. 2. Water/silicone oil system. Neutral stability curves. Critical Rayleigh number vs. dimensionless wave number α, at (a) lower liquid depths $l_1 = 0.61$ (- -), 0.62 (-.), 0.63 (line), (b) 0.64 (- -), 0.65 (-.), 0.66 (line), (c) 0.67 (- -), 0.68 (-.), 0.69 (line), (d) 0.7 (- -), 0.71 (line).

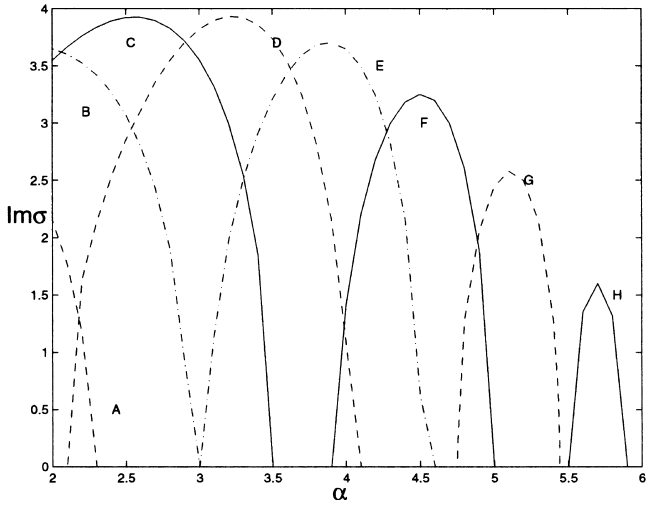

Fig. 3. Water/silicone oil system. Im σ vs. dimensionless wave number α along neutral stability curves, at lower liquid depths $l_1 = 0.63$ (A), 0.64 (B), 0.65 (C), 0.66 (D), 0.67 (E), 0.68 (F), 0.69 (G), 0.7 (H).

and 3, we would expect to see the oscillations induced at lower liquid depths 0.67 and 0.71. The available data concerning the oscillations are shown in their Fig. 21 for depth 0.71, which plots the primary oscillation period and primary wave numbers. We need more information than currently available, such as graphs of the power spectral density for their signals or some form of Fourier Transform of their observed periods, to interpret the experiments in light of

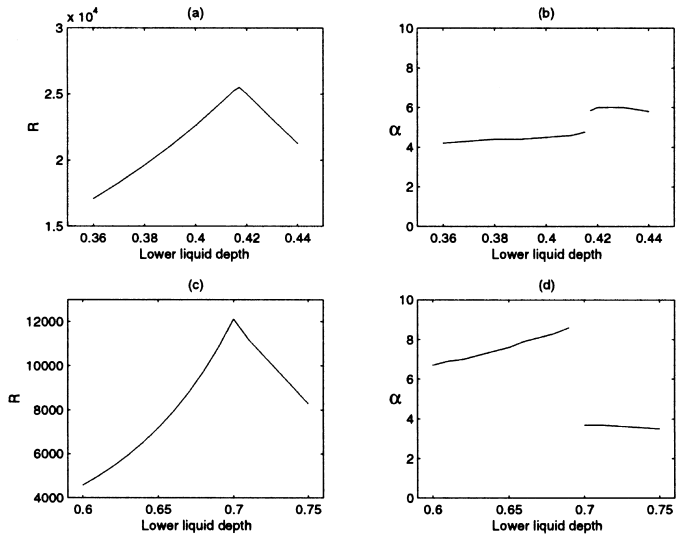

Fig. 4. (a) Fluorinert/silicone oil system. Critical Rayleigh number vs. dimensionless lower liquid depth l_1. (b) Fluorinert/silicone oil system. Critical values for dimensionless wave number α vs. dimensionless lower liquid depth l_1. (c) Water/silicone oil system. Critical Rayleigh number vs. dimensionless lower liquid depth l_1. (d) Water/silicone oil system. Critical values for dimensionless wave number α vs. dimensionless lower liquid depth l_1.

the theory. Such graphs would show more clearly the relative strengths of the periods that are observed. Our interpretation of the data given for depth 0.71 is that at the Rayleigh number of 21,500, it is possible for the recorded wave number around 11, corresponding to a trough of the neutral stability curve, to be unstable, as well as its subharmonic at wave number 5.5, which is close to a time-periodic mode. If the lower liquid depth were .01 or .02 less, then there would be a resonance of the steady mode at wave number 11 with a subharmonic mode at wave number 5.5 which is time periodic with the period lying in the range shown in Fig. 22 of Degen et al. (1998). There is some scatter in their Fig. 22 and periods range from 15 to 40 min.

The onset mode at each depth fraction is shown in Fig. 4 and are steady. However, when the Rayleigh number is increased slightly above onset, especially around $l_1 = 0.7$, the Hopf modes become unstable as well.

Around $l_1 = 0.69$, the critical Rayleigh number is almost independent of wave number over a wide range of wave numbers, complicating a full theoretical analysis. Time-periodic oscillations around wave number 5 to 6, and steady modes around wave number 4, as well as from 10 to 11, are unstable under experimental conditions. When the Rayleigh number is pushed above onset, the fastest growing modes are those at wave numbers 10 to 11. At $l_1 = 0.69$, The $\mathrm{Im}\,\sigma$ maximum is 2.6, yielding a period of 47 min. At $l_1 = 0.7$, $\mathrm{Im}\,\sigma_{\max} = 1.6$, giving 77 min.

As l_1 decreases to around 0.62, the oscillatory modes move to longer wavelengths which have much higher critical Rayleigh numbers (cf. Fig. 3).

2.1.2. Temperature contours

From lower liquid depths of 0.60–0.69, the perturbation temperature field for the onset mode is dominant in the top layer. At lower liquid depths of 0.70–0.75, the perturbation temperature field consists of one large roll covering both layers.

At $l_1 = 0.7$, the neutral stability curve of Fig. 2 shows a unique situation, where more than one wave number would in practice become unstable together. Specifically, at wave number 3.7, the critical Rayleigh number is 12,119 while at wave number 8.9, it is 12,135. For the critical curves in Fig. 4, we have chosen strictly the lowest onset Rayleigh number and corresponding wave number. Depth 0.7 also has the oscillatory modes becoming unstable at wave numbers 5.6–5.8, with 5.8 at Rayleigh number 14,868. These Rayleigh numbers occur for temperature variations of less than 0.5°C, while experimental data were taken slightly above this. The behavior described above for depth fractions 0.70–0.75 can be explained by the presence of two troughs in the neutral stability curves. For the trough with the higher wave numbers, the perturbation temperature field is dominant in the top layer.

As evidenced by the neutral stability curves in Fig. 2, depth fractions between 0.62 and 0.70 possess oscillatory onsets. For wave numbers slightly less than those of the oscillatory range, the temperature field consists of a large roll covering both layers as shown in Fig. 5(a) at wave number 5.4. At the mode with the maximum $\mathrm{Im}\,\sigma$, the perturbation temperature field consists of linked rolls between the two layers as shown in Fig. 5(b) for wave number 5.7. Slightly above the wave number for oscillations, the perturbation temperature field consists of rolls in each fluid as shown in Fig. 5(c) at wave number 6. For higher wave numbers, the roll in the top begins to dominate.

The overall behavior of the perturbation temperature field has four stages as the wave number increases from steady modes, through time-periodic modes, then back to steady

modes: (1) a single large roll over the entire depth as in Fig. 5(a), (2) a linked roll as in Fig. 5(b), (3) separate rolls in each layer as in Fig. 5(c), and (4) roll in the top fluid only.

2.1.3. Velocity field

For those depths that possess oscillatory onsets, three distinct patterns emerge: thermal coupling, mechanical coupling, and a transition state that exists as a blend of the two types of coupling. (For definitions of thermal and mechanical coupling, we refer the reader to Degen et al. (1998), Busse and Sommermann (1996), Rasenat et al. (1989) and Andereck et al. (1996)). For depth fractions from 0.65 to 0.70, a distinct three-step pattern is evident as the wave number increases: (1) at wave numbers less than those of the Hopf region, thermal coupling as in Fig. 6(a), (2) at wave numbers in the Hopf region, transition state as in Fig. 6(b), (3) at wave numbers greater than those of the Hopf region, mechanical coupling as in Fig. 6(c). These results are summarized in Table 1.

2.2. The Fluorinert/silicone oil 47v10 system

For the Fluorinert/silicone oil 47v10 system, the plate separation is taken as 1.26 cm, $P = 406.3$, $\beta = 0.93$, $\gamma = 0.40$, $r = 2.09$, $\zeta = 0.54$, $m = 2.93$, $G = (RP)/(\hat{\alpha}_1 \Delta T) = 1.7 \times 10^{10}$. For an interfacial tension of 7 dyn/cm (Burkersroda et al., 1994). $S = 94.2 \times 10^3$. The linear stability results change very little with change in interfacial tension (at 20 dyn/cm, the results are essentially the same). The experimental measurements in Fig. 3.16 and Fig. 3.17 of Degen (1997) show that at depth $l_1 = 0.375$, oscillations are recorded for $\alpha = 5.2$, with periods between 45 and 80 min. The experiments were performed for Rayleigh numbers 36,000 and larger. The linear theory predicts that steady modes become unstable at wave number 5.2, as shown in Fig. 4.

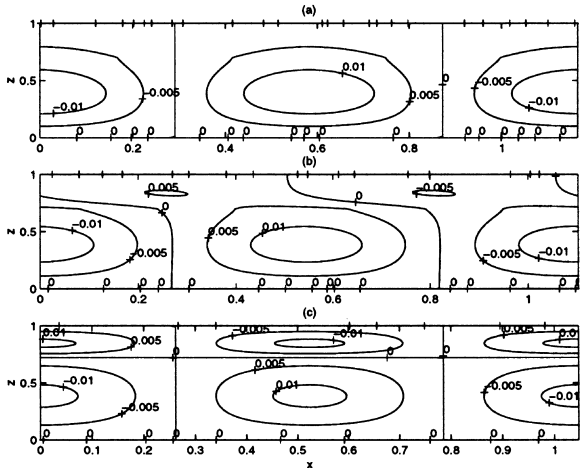

Fig. 5. Water/silicone oil system. Perturbation temperature contour plots for dimensionless lower liquid depth $l_1 = 0.7$. Oscillations occur at dimensionless wave numbers $\alpha = 5.6$–5.8. (a) Wave number 5.4. Steady mode. (b) Wave number 5.7. Oscillatory mode. (c) Wave number 6. Steady mode.

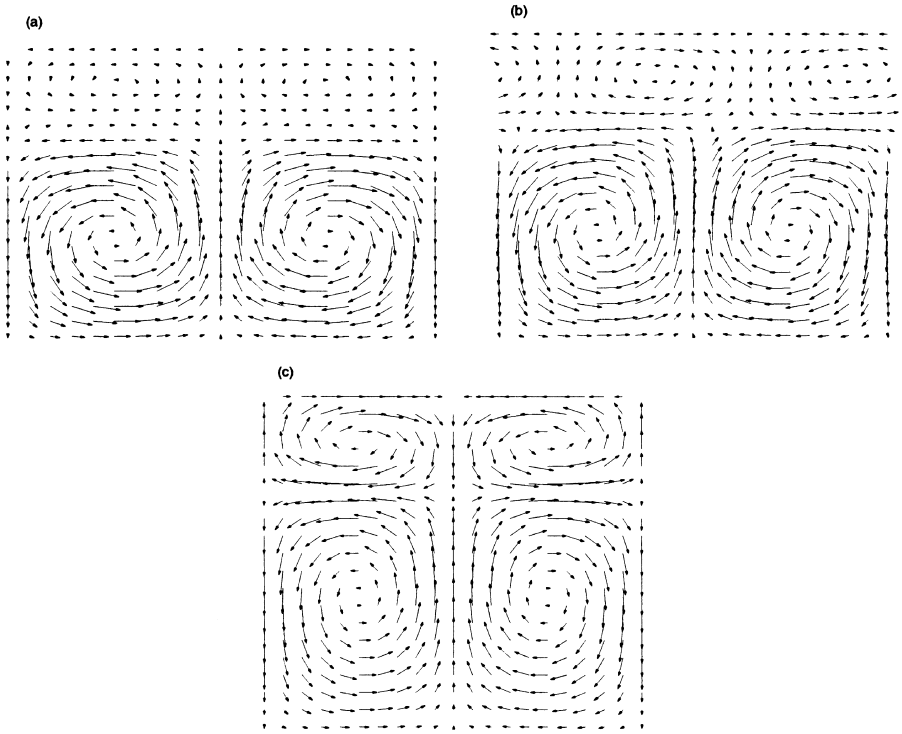

Fig. 6. Water/silicone oil system. Velocity vector plots at dimensionless lower liquid depth $l_1 = 0.69$, showing trends in the location of the rolls as the wave number passes through the Hopf range. (a) $R = 13{,}823$. Dimensionless wave number $\alpha = 4.5$. Rolls are thermally coupled. (b) $R = 14{,}205$. Wave number 5.2, inside the Hopf range. Rolls are in a transition regime. (c) $R = 12{,}817$. Wave number 5.9, greater than those of the Hopf range. Rolls are mechanically coupled. A summary of behavior at other depth fractions is given in Table 1. The plots extend one wavelength in the x-direction, and over $z = 0$ to 1 vertically.

Table 1
Summary of velocity vector field behavior for water/silicone oil system for depth fractions 0.65–0.70[a]

l_1	α		
	Thermal coupling	Transition	Mechanical coupling
0.62	NA	0.9	2.0
0.63	NA	1.5	2.5
0.64	NA	2.6	3.0
0.65	1.0	2.8	4.0
0.66	2.0	3.3	4.5
0.67	2.5	4.0	5.0
0.68	3.5	4.5	5.5
0.69	4.5	5.2	5.9
0.70	5.4	5.7	6.0

[a] Data taken at wave number less than Hopf range (thermally coupled rolls), inside the Hopf range (transition regime), and greater than Hopf range (mechanically coupled rolls). The velocity fields are illustrated in Fig. 6.

2.2.1. Neutral stability curves

The neutral stability curves in Figs. 7 and 8 illustrate that there is a small interval of wave numbers from 3.2 to 4.2 at the lower liquid depth of 0.43 which are oscillatory.

2.2.2. Temperature contours

Perturbation temperature contour plots are shown in Figs. 9 and 10. For the critical mode at $l_1 = 0.36$–0.40, the roll in the upper layer is dominant, with little going on in the bottom layer, as shown in Fig. 9(a) for depth 0.36. The convection in the bottom layer begins to increase as the depth fraction changes from 0.36 to 0.40 (cf. 9(b) for depth 0.41). A transition takes place between lower liquid depths 0.41 and 0.42, and for depths 0.42 to 0.44, the dominant temperature field of the onset mode is in the bottom layer, as shown in Fig. 9(c).

We next examine the oscillatory regime at depth 0.43. Oscillatory onsets occur along the neutral stability curve at $l_1 = 0.43$ for wave numbers 3.2–4.2, a very narrow range. For a wave number slightly less than 3.2 (see Fig. 10(a) at $\alpha = 3$) the motion consists of steady rolls in the upper layer. Within the oscillatory regime, (see Fig. 10(b) at $\alpha = 3.7$), contours of the perturbation temperature field are joined for both layers in the shape of linked rolls. Slightly above wave number 4.2 (see Fig. 10(c) at $\alpha = 5$) the motion is dominated by steady rolls in the bottom fluid. Thus, the temperature field is dominant in one of the fluids, not both, as the oscillatory regime is approached, and the rolls then become of equal magnitude in both layers within the oscillatory regime.

2.2.3. Velocity field

Unlike the water/silicone system, at wave numbers less than those of the Hopf region, the

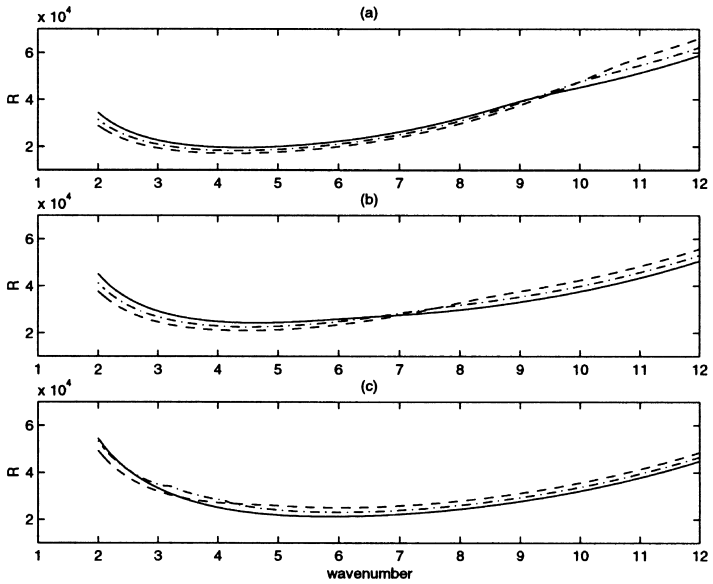

Fig. 7. Fluorinert/silicone oil 47v10 system. Neutral stability curves for the onset modes at dimensionless lower liquid depths l_1 = (a) 0.36 (- -), 0.37 (-.), 0.38, (b) 0.39 (- -), 0.40 (-.), 0.41, (c) 0.42 (- -), 0.43 (-.), 0.44. Plots show critical Rayleigh number vs. dimensionless wave number α.

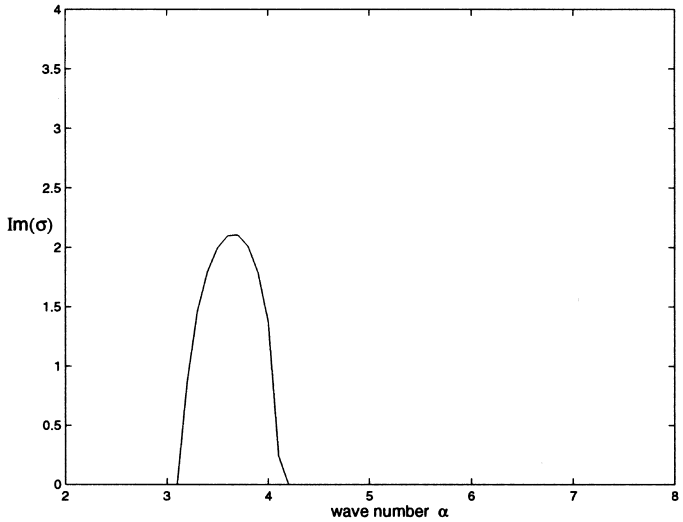

Fig. 8. Fluorinert/silicone oil 47v10 system. Imaginary part of eigen-value σ vs. dimensionless wave number α, along neutral stability curve at lower liquid depth $l_1 = 0.43$, showing oscillatory onsets. The other depths shown in Fig. 7 have real onsets, not oscillatory.

system exhibits moderate mechanical coupling, not thermal coupling, as shown in Fig. 11(a). At wave numbers less than those of the Hopf region, the motion takes place almost entirely in the top layer of fluid, and so the mechanical coupling behavior may not be detectable experimentally. In the Hopf region, the system is in transition as shown in Fig. 11(b), and at wave numbers greater than those of the Hopf region, mechanical coupling is once again evident, as shown in Fig. 11(c).

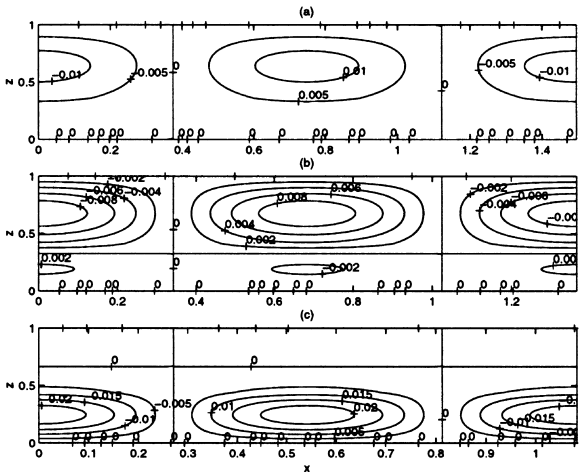

Fig. 9. Fluorinert/silicone oil system. Perturbation temperature contour plots for steady critical modes. (a) Dimensionless lower liquid depth $l_1 = 0.36$, dimensionless wave number $\alpha = 4.2$. (b) $l_1 = 0.41$, wave number 4.6. (c) $l_1 = 0.44$, wave number 5.8.

3. Hopf bifurcation in 3D

The group of Degen et al. (1998) has on-going plans to do experiments in larger cells, and this motivated a theoretical analysis for solutions which are doubly periodic with respect to a hexagonal lattice. Other types of spatial periodicities such as square (Tokaruk et al., 1998) or rhombic are equally worth investigating. The symmetry of the hexagonal lattice causes a sixfold degeneracy of the critical eigenvalue. Hopf bifurcations of this type have been investigated extensively (Roberts et al., 1986; Renardy and Renardy, 1988; Joseph and Renardy, 1993), and we merely present results here. There are eleven qualitatively different types of bifurcating solutions: standing rolls, standing hexagons, standing regular triangles, standing patchwork quilt, travelling rolls, travelling patchwork quilt of type 1, travelling patchwork quilt of type 2, oscillating triangles, wavy rolls of type 1, wavy rolls of type 2, and twisted patchwork quilt. The visualization of these states, for the reader unfamiliar with them, is given in the color plates of Joseph and Renardy (1993). Table 2 lists the stable solutions which we found. Traveling rolls, wavy rolls of type 1, and oscillating triangles appear in each system. The water/silicone oil system also exhibits the traveling patchwork quilt of type 2 for three situations, which are at the low wave number side of the Hopf range for lower liquid depths 0.62, 0.65 and 0.66. At the lower end of the depth fractions, 0.62 and 0.63 show a preference for travelling rolls. As the depth fraction increases, more exotic solutions such as the wavy rolls of type 1, and oscillating triangles also appear. At depth fraction 0.7 which is the largest depth fraction displaying a Hopf range, oscillating triangles are stable for wave numbers throughout the Hopf regime.

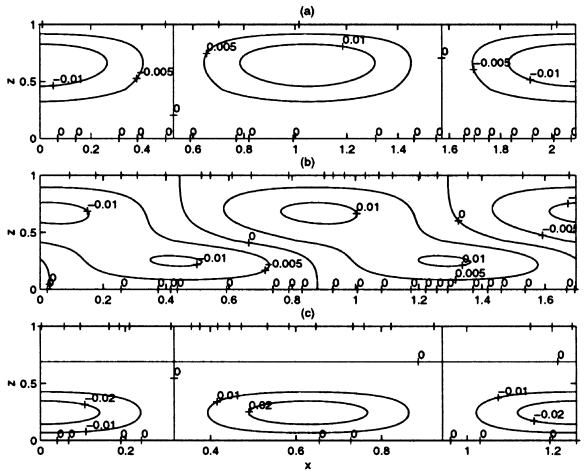

Fig. 10. Fluorinert/silicone oil system. Perturbation temperature contour plot of critical mode. Dimensionless lower liquid depth $l_1 = 0.43$. (a) Steady mode at wave number $\alpha = 3.0$, slightly less than oscillatory onset shown in Figs. 7 and 8. (b) Wave number 3.7 at oscillatory onset shown in Fig. 8. (c) Steady mode at wave number 5.0, slightly more than oscillatory onset shown in Fig. 8.

4. Conclusion

We have investigated two specific systems, motivated by experimental observations (Degen et al., 1998). The first is composed of silicone oil Rhodorsil 47v2 lying over water. Experimental data by Degen et al. (1998) were taken around depth fraction 0.6–0.71. Recorded periods at depth fraction 0.71 show a primary period around 25 min, with scatter up to 40 min. The primary wave number is 10 with scatter from 1 to 80. Our linearised stability analysis at depth fraction 0.7 predicts the largest growth rate modes are (i) steady modes of wavenumber 4 to 5,

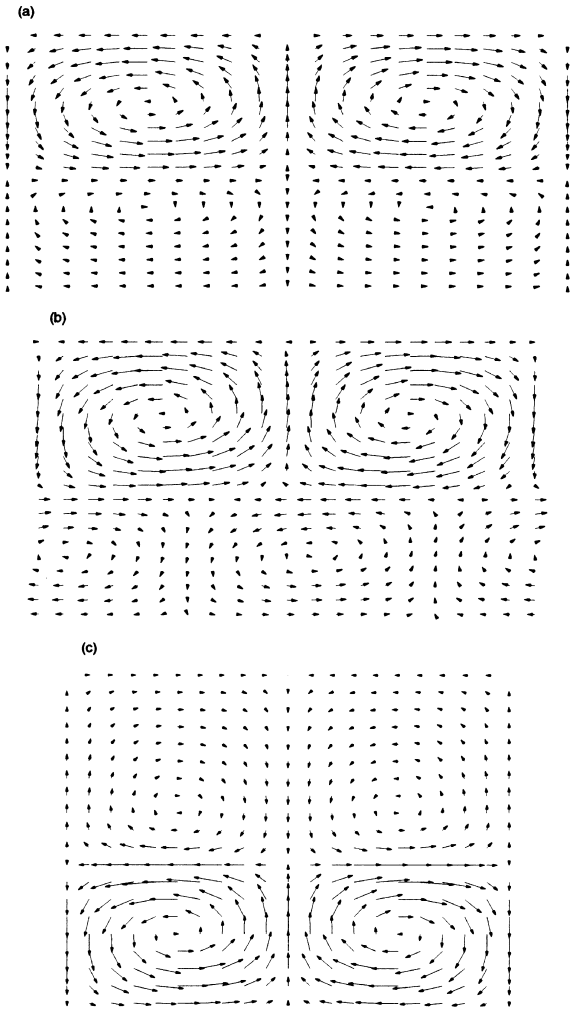

Fig. 11. Fluorinert/silicone oil system. Velocity vector plots at dimensionless lower liquid depth $l_1 = 0.43$, showing trends in the location of the rolls. (a) $R = 34{,}959$. Wave number $\alpha = 3.0$, less than the Hopf range. Rolls are moderately mechanically coupled. (b) $R = 30{,}065$. Wave number 3.7, inside the Hopf range. Rolls are in a transition regime. (c) $R = 24{,}044$. Wave number 5.0, greater than the Hopf range. Rolls are mechanically coupled. The plots show one wavelength in the x-direction and z extending from 0 to 1.

(ii) steady modes 9 to 10, and (iii) oscillatory modes, period 50 min at wave number 5.4. Much of the action occurs in the water layer for the oscillatory range and for the steady modes around wave number 5, but the higher wave number around 10 induces roll action in the top layer. Experimental visualisation is stated to be difficult in the lower water layer (Degen, 1997); thus, one possibility is that wave number 11 was observed in the upper layer representing the steady mode, which has a wavelength half that of the oscillatory mode (Fig. 22(b) of Degen et al. (1998); records some secondary wave numbers in this range), together with a record of the oscillation period for wave number 5.5. There is high sensitivity to the depth fraction. At depth fraction 0.69, the period shortens to 30 min, and at depth 0.68–25 min. Therefore, we suggest that controlled experiments be aimed at lower liquid depths 0.65 to 0.68 and at a specific wave number targetting the oscillatory range. Even at these depths, it is likely that a band of wave

Table 2
Pattern formation results for water/silicone oil system and Fluorinert/silicone oil system

l_1	R	α	$\lvert\mathrm{Im}\,\sigma\rvert$	Stable solution
Water–silicone oil system				
0.62	880328	0.3	2.3	Traveling patchwork quilt (2)
	500657	0.4	2.2	Traveling rolls
	226181	0.6	2.0	Traveling rolls
	103236	0.9	1.7	Traveling rolls
0.63	91186	1	3.2	Traveling rolls
	43246	1.5	3	Traveling rolls
	22823.7	2.2	1.17	Traveling rolls
0.64	120035	0.9	3.3	Traveling rolls and wavy rolls (1)
	33947	1.8	3.7	Traveling rolls
	19184	2.6	2.8	Oscillating triangles
0.65	74985	1.2	2.1	Traveling patchwork quilt (2)
	18601	2.8	3.8	Wavy rolls (1) and oscillating traingles
	15237	3.3	2.5	Wavy rolls (1) and oscillating triangles
0.66	26314	2.3	2.1	Traveling patchwork quilt (2)
	16295	3.3	3.9	Wavy rolls (1) and oscillating triangles
	14146	3.8	2.8	Traveling rolls and wavy rolls (1)
0.67	18008	3.2	1.98	Oscillating triangles
	14458	4	3.6	Traveling rolls and wavy rolls (1)
	13499	4.4	1.6	Oscillating triangles
0.68	15119	4.1	2.2	Traveling rolls
	14202	4.5	3.2	Traveling rolls and wavy rolls (1)
	13728.5	4.8	2.6	Traveling rolls and wavy rolls (1)
0.69	14506.8	4.9	2.06	Traveling rolls
	14205	5.2	2.5	Traveling rolls and wavy rolls (1)
	14068	5.4	1.3	Oscillating triangles
0.70	14918	5.6	1.3	Oscillating triangles
	14888	5.7	1.6	Oscillating triangles
	14868	5.8	1.3	Oscillating triangles
Fluorinert–silicone oil system				
0.43	30065	3.7	2.1	Traveling rolls and wavy rolls (1)
	28512	4	1.4	Oscillating triangles

numbers are unstable together, but at least these do not suffer from two troughs in the neutral stability curves.

The second system is composed of silicone oil Rhodorsil 47v10 lying on Fluorinert. We find that oscillatory instabilities are possible, but in a much narrower range of parameters than in the silicone oil/water system. The experimental data of Degen et al. (1998) recorded oscillations of roughly the same wave number and period as we predict but the depth fraction is slightly different and observations were above criticality. This study raises the following questions for future experimental consideration: whether the width of the experimental cell affects the critical conditions, and whether the values of the physical properties of the fluids, such as viscosity, need to be re-measured. Oscillations are predicted at a higher Rayleigh number than criticality, but if the wave number is restricted, then the oscillations would be the critical modes, just as in the water/silicone oil system. For both systems, therefore, experiments for oscillatory onsets need to be seeded for specific wave numbers.

A theoretical model for steady onset, followed by oscillations at slightly higher Rayleigh number, is given by Renardy et al. (1999). Time-periodic solutions, which have been analyzed for the Hopf bifurcation case (see Section 3), again arise, but some can now be excited as a secondary bifurcation from steady solutions rather than as a bifurcation directly from the rest state. For the Fluorinert/silicone oil system, a temporally chaotic regime with triangular spatial symmetry is predicted. Whether these patterns would be observable in experiments remains to be investigated.

Acknowledgements

This research was sponsored by the National Science Foundation under Grant No. CTS-9612308.

References

Andereck, C.D., Colovas, P.W., Degen, M.M., 1996. Observations of time-dependent behavior in the two-layer Rayleigh–Benard system. In: Renardy, Y.Y., Coward, A.V., Papageorgiou, D., Sun, S.-M. (Eds.), Advances in Multi-Fluid Flows. SIAM, Philadelphia, pp. 3–12.

Andereck, C.D., Colovas, P.W., Degen, M.M., Renardy, Y.Y., 1998. Instabilities in two-layer Rayleigh–Benard convection: overview and outlook. Int. J. Eng. Sci 36, 1451–1470.

Burkersroda, C.V., Prakash, A., Koster, J.N., 1994. Interfacial tension between Fluorinert liquids and silicon oils. Microgravity Q 4, 93–99.

Busse, F.H., Sommermann, G., 1996. Double-layer convection: a brief review and some recent experimental results. In: Renardy, Y.Y., Coward, A.V., Papageorgiou, D., Sun, S.-M. (Eds.), Advances in Multi-Fluid Flows. SIAM, Philadelphia, pp. 33–41.

Colinet, P., Legros, J.C., 1994. On the Hopf bifurcation occurring in the two-layer Rayleigh–Benard convective instability. Phys. Fluids 6, 2631–2639.

Degen, M.M., 1997. Ph.D. dissertation. The Ohio State University.

Degen, M.M., Colovas, P.W., Andereck, C.D., 1998. Time-dependent patterns in the two-layer Rayleigh–Benard system. Phys. Rev. E 57, 6647–6659.

Fujimura, K., Renardy, Y., 1995. The 2:1 steady-Hopf mode interaction in the two-layer Benard problem. Physica D 85, 25–65.

Gershuni, G.Z., Zhukhovitskii, E.M., 1976. Convective Stability of Incompressible Fluids. Keter, Jerusalem.

Johnson, D., Narayanan, R., 1997. Geometric effects on convective coupling and interfacial structures in bilayer convection. Phys. Rev. E 56, 5462–5472.

Johnson, D., Narayanan, R., 1998. Marangoni convection in multiple bounded fluid layers and its application to materials processing. Phil. Trans. R. Soc. Lond A 356, 885–898.

Johnson, D., Naryanan, R., Dauby, P.C., 1998. The Effect of Air Height on the Pattern Formation in Liquid–Air Bilayer Convection, preprint.

Joseph, D.D., Renardy, Y.Y., 1993. Fundamentals of Two-Fluid Dynamics. Springer-Verlag, New York.

Rasenat, S., Busse, F.H., Rehberg, I., 1989. A theoretical and experimental study of double-layer convection. J. Fluid Mech 199, 519–540.

Renardy, M., 1996a. Hopf bifurcation on the hexagonal lattice with small frequency. Advances in Diff. Eq 1, 283–299.

Renardy, Y., 1996b. Pattern formation for oscillatory bulkmode competition in a two-layer Benard problem. Z. Angew. Math. Phys. 47, 567–590. Errata 1997 48, 171.

Renardy, M., Renardy, Y., 1988. Bifurcating solutions at the onset of convection in the Benard problem for two fluids. Physica D 32, 227–252.

Renardy, Y.Y., Renardy, M., Fujimura, K., 1999. Takens–Bogdanov bifurcation on the hexagonal lattice for double-layer convection. Physica D 129, 171–202.

Renardy, Y., Stoltz, C.G., 1999. Time-dependent pattern formation for two-layer convection. In: Golubitsky, M., Luss, D., Strogatz, S. (Eds.), Pattern Formation in Continuous and Coupled Systems, IMA Volumes in Mathematics and its Applications, vol. 115. Springer-Verlag, New York, pp. 203–214.

Roberts, M., Swift, J.W., Wagner, D.H., 1986. The Hopf bifurcation on a hexagonal lattice. AMS Contemp. Math 56, 283–318.

Tokaruk, W.A., Molteno, T.C.A., Morris, S.W., 1998. Benard–Marangoni convection in two layered liquids, preprint.